CO_2 Capture

DOI: 10.1002/anie.201202992

Low-Energy Selective Capture of Carbon Dioxide by a Pre-designed Elastic Single-Molecule Trap**

*Mario Wriedt, Julian P. Sculley, Andrey A. Yakovenko, Yuguang Ma, Gregory J. Halder, Perla B. Balbuena, and Hong-Cai Zhou**

Carbon capture and sequestration (CCS) has been proposed as a means to mediate anthropogenic carbon dioxide emissions and has received a considerable amount of research attention in the last decade.[1] The most energy- and cost-intensive aspect of carbon capture is removing carbon dioxide from flue gas streams of power plants, because the state-of-the-art amine-scrubbing technology places an enormous parasitic demand on the power plant during sorbent regeneration.[2] Metal–organic frameworks (MOFs) have received considerable attention because the rational design[3] employed in their construction promises materials that are tailored to specific needs.[4] The difficulty in using materials to selectively physisorb CO_2 from flue gas lies in precisely tuning sorption interactions to only CO_2.[5] Herein we report the use of a novel strategy for tuning MOFs to recognize specific guest molecules, creating a new class of thermally and chemically stable physisorptive materials. The first in this class is a guest-responsive MOF (PCN-200; PCN = porous coordination network) that has been rationally designed to capture CO_2 over N_2 under flue gas conditions by an elastic-binding mechanism[6] while the low heat capacities significantly reduce the overall energy needed for regeneration. We established this elastic CO_2 trapping effect of PCN-200 using four independent methods: single-component gas-adsorption isotherms, binary gas adsorption studies by simulations and experiments, and crystallographic determination of the adsorbed gas. Through molecular-level control of a material, our results demonstrate the design and synthesis of a new class of low-energy CO_2 sorbents.

It has been proposed that by shifting focus from energy consuming aqueous alkanolamine solutions to physisorptive materials, the estimated cost of CCS (70% of which is derived from the capture step) can be drastically lowered through materials optimization.[7] Previously, we synthesized mesh-adjustable molecular sieves (MAMS) capable of adsorbing specific gas molecules in a narrow temperature range through designed stimuli-responsive gating effects.[8] These materials were constructed of weakly bonded (van der Waals interactions, vdW) sheets with one-dimensional gated channels. The problem of applying these materials to harsh flue gas applications lays primarily in the stability of the intersheet bonding interactions. Herein we report the rational design of the next generation material, in which this problem is overcome by introducing strong coordination bonds between the layers. The vast choice of ligands was narrowed down to a short interlayer distance to fit exactly one CO_2 molecule into the elastic polar pocket of PCN-200 while designing CO_2 specific interactions. The resulting multipoint bonding of CO_2 to a precisely designed pocket is reminiscent of the biomimetic recognition employed by receptors in nature to accommodate exactly one guest molecule.

The framework organizing these traps in space, $[Cu(tzc)(dpp)_{0.5}]_n \cdot 1.5\,H_2O$ (PCN-200-syn, tzc = tetrazolate-5-carboxylate, dpp = 1,3-di(4-pyridyl)propane), has proper Cu···Cu distances in the direction of the *b* axis to form CO_2 pockets, controlled by μ_3-bridging tzc ligands forming layers in the *bc* plane (Figure 1b). The flexible N-donor linker dpp (Fig-

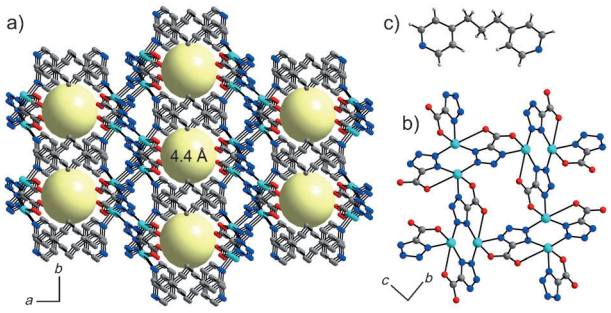

Figure 1. Crystal structure of PCN-200-ac and its components: a) perspective view along the *c* axis; b) orthographic view on a single $[Cu(tzc)]_n$ layer along the *a* axis; c) the flexible N-donor linker 1,3-di(4-pyridyl)propane.

[*] Dr. M. Wriedt, J. P. Sculley, A. A. Yakovenko, Prof. Dr. H.-C. Zhou
Department of Chemistry, Texas A&M University
College Station, TX 77843 (USA)
E-mail: zhou@chem.tamu.edu
Homepage: http://www.chem.tamu.edu/rgroup/zhou/
Dr. G. J. Halder
X-ray Science Division, Advanced Photon Source
Argonne National Laboratory
Argonne, IL 60439 (USA)
Dr. Y. Ma, Prof. Dr. P. B. Balbuena
Artie McFerrin Department of Chemical Engineering
Texas A&M University
College Station, TX 77843 (USA)

[**] Funding was provided by the U.S. Department of Energy (DOE DE-SC0001015 and DE-AR0000073). M.W. acknowledges the Postdoc Programme of the German Academic Exchange Service (DAAD) for his financial support. Special thanks go to C. Näther from the University of Kiel (Germany) for the crystallographic help on PCN-200-syn and A. Callejas-Tovar who carried out the IAST calculations. Use of the Advanced Photon Source, an Office of Science User Facility operated for the U.S. Department of Energy (DOE) Office of Science by Argonne National Laboratory, was supported by the U.S. DOE under Contract No. DE-AC02-06CH11357. In this context we thank K. W. Chapman for her onsite help.

Supporting information for this article is available on the WWW under http://dx.doi.org/10.1002/anie.201202992.

ure 1c) provides the strong interlayer bonds that connect these layers into a 3D network forming 1D pores along the *c* axis with the center of the pores located on a center of inversion (Figure 1a). Recent investigations of compounds based on the same tzc ligand with similar N-donor ligands 4,4′-bipyridine[9] and 1,2-di(4-pyridyl)ethane[10] are nonporous; in the latter case, the tzc layer intersheet distances are too short.[10] Thus, we chose the dpp ligand to ensure the correct intersheet distance to accommodate exactly one CO_2 molecule, while the flexibility of the linking propylene chain was used to gain the advantageous elastic trapping effect.[11] In the as-synthesized structure, non-coordinating water molecules occupy the pores (Figure 4b, bottom) and are stabilized by strong hydrogen bonding (Supporting Information, Section S2). The water molecules of the precursor compound PCN-200-syn can be easily removed by either heating to 80 °C or applying vacuum (10 μbar, 5 min), leading to the activated phase $[Cu(tzc)(dpp)_{0.5}]_n$ (PCN-200-ac; Figure 1a, Figure 4b, middle). This activation process is accompanied by a phase transition keeping the same space group (*C*2/*c*), almost the same unit cell length parameters, but a dramatic change in the unit cell angle β, from 92.657(10)° in PCN-200-syn to 116.087(4)° in PCN-200-ac. The crystal structure of PCN-200-ac was solved from in situ synchrotron-based powder diffraction (SPD) patterns and refined by the Rietveld method (Supporting Information, Section S3). Owing to the elastic nature of the dpp ligand, the pores opened up to where the largest vdW sphere has a diameter of 4.4 Å, which can be used to fit exactly one gas molecule per pore (Supporting Information, Section S3).

PCN-200-ac is stable up to 218 °C, which meets the temperature requirements for physical sorbents in a flue gas separation process (Supporting Information, Section S4). Chemical stability tests show that PCN-200 is stable after stirring in HCl (pH 2) and NaOH (pH 12) and boiling in water for 7 days while retaining porosity, which further confirms the substantially stronger intersheet stability afforded by the nitrogen–copper bonds (Supporting Information, Figure S11).

The thermal and chemical stability concerns that have plagued other MOFs have been addressed by the aforementioned experiments. However, to show that the material will be useful in practical applications, it must also compete with all other porous materials in terms of gas uptake and selectivity. To show that PCN-200 can selectively adsorb CO_2 over N_2 in a practical setting, it was evaluated from four mutually independent, well-established techniques: single-component gas-adsorption isotherms, binary gas-adsorption studies by simulations and experiments, and crystallographic determination of the adsorbed gas, the results of which all confirm high selectivity. The first technique is using experimental single-component gas isotherms to examine loading capacities of CO_2 and N_2 at various temperatures (Figure 2; Supporting Information, Section S5). The completeness of the activation procedure is clearly shown by the CO_2 uptake at 195 K, which reaches full saturation of 4 molecules per unit cell (1.78 mmol g^{-1}) at 1 bar. Simulated single gas isotherms are in excellent agreement with these experimental observations (Supporting Information, Figure S23). An additional

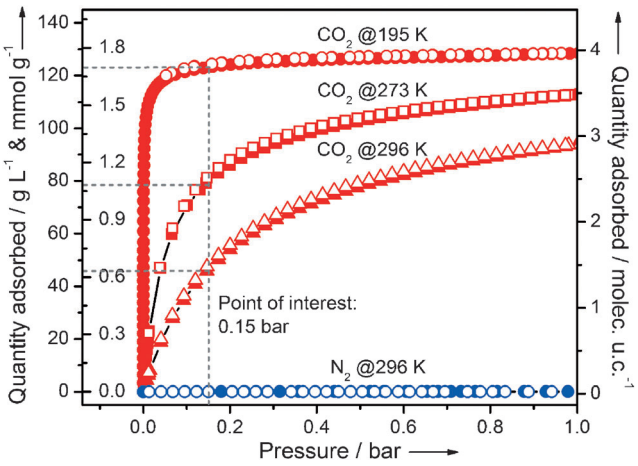

Figure 2. Gas adsorption isotherms for CO_2 and N_2 of PCN-200-ac. CO_2 at 195 K (red circles), 273 K (rectangles), 296 K (triangles) and N_2 at 296 K (blue circles). The filled and open symbols represent adsorption and desorption, respectively, and the gray dashed lines indicate the adsorption values at 0.15 bar (partial pressure of CO_2 in flue gas with typical composition of 14–16% CO_2 and 75% N_2).

consideration that must be taken into account is the volumetric storage capacities, as the volume of the adsorbent plays a significant role in industrial-scale applications.[2b] The exceptionally high density of PCN-200-ac (1.64 g mL^{-1}) compared to other MOFs (Supporting Information, Table S8) leads to a high uptake capacity of 129 g L^{-1}. More importantly, the material retains 75% of its uptake capacity at ambient conditions. Even after running a series of thirty adsorption–desorption cycles at 313 K, emphasizing the conditions of real flue gas, there was no loss in capture capacity (Supporting Information, Figure S17).

To quantify the adsorption affinities, we used two common methods,[5b] namely fitting experimental gas isotherms using both the virial and Langmuir equations and calculating zero-coverage heats of adsorption (−38 kJ mol^{-1} and −49 kJ mol^{-1}, respectively; Supporting Information, Section S7). These values fall well within the range of what is considered to be an ideal adsorption enthalpy for CO_2 scrubbing from flue gas. Adsorption enthalpies that are too low translate to low selectivities, while higher enthalpies will raise regeneration costs because of the energy input required for the reverse process. Recent studies have shown that a temperature swing adsorption (TSA) regeneration process would be significant less energy consuming than pressure swing adsorption (PSA) and thus, more applicable in a real world application scenario for CO_2 capture from flue gas.[12] In this context, the high-energy requirement for the regeneration of aqueous amine solutions stems from the high adsorption enthalpies of chemisorption (−50 to −100 kJ mol^{-1}) and the high heat capacity of the aqueous amine solution (ca. 3.5 J g^{-1} K^{-1}),[13] whereas the heat capacity of PCN-200 is only one third of that value (Supporting Information, Figure S16). Therefore, a combination of moderate heats of adsorption and low heat capacity of PCN-200 will lead to low regeneration energies in comparison with state of the art technologies. Because of their modular design,

MOFs have been tuned to selectively capture CO_2 through the incorporation of unsaturated metal centers or polar functional groups.[12,14] The difference in our approach is that we do not use any high-enthalpy adsorption interactions. We instead created a polar pocket that traps CO_2 and excludes other gas molecules; the moderate heat of adsorption results from a combination of polar pore surface and pore size. By controlling guest-framework interactions, we designed a material that requires very little energy to regenerate, yet has extremely high selectivity for CO_2. The precise design of the CO_2 trap thus leads to a remarkably high adsorption enthalpy for a purely physisorptive material (Supporting Information, Table S8).

The second technique, annealing simulations, shows that both gas molecules compete for the adsorption site at the center of the pocket leading to selectivity values of 260 (50:50) and 205 (15:85) for binary CO_2/N_2 mixtures at 296 K and 1 bar according to our grand-canonical Monte Carlo (GCMC) simulations (Supporting Information, Section S6).

The high CO_2/N_2 selectivity of PCN-200 can be confirmed by binary gas-adsorption experiments, the third technique. Figure 3 presents the dynamic cycling behavior of temperature dependent gravimetric adsorption studies using a TGA. After heating PCN-200 at 150 °C for 20 min, the sample was

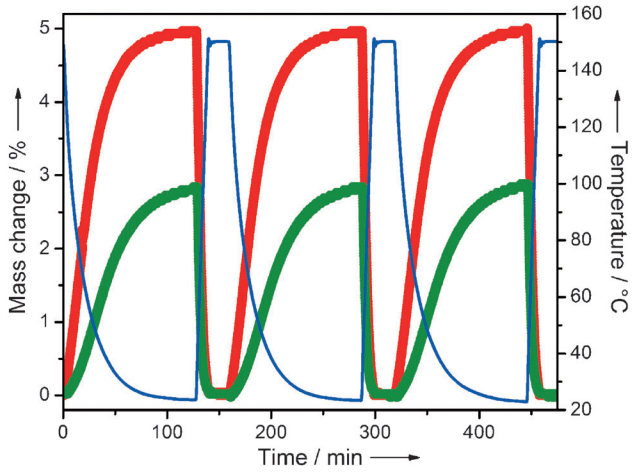

Figure 3. Temperature-dependent gravimetric adsorption studies of PCN-200-ac using TGA. Experimental mass changes are shown as a function of temperature in pure CO_2 (red circles) and CO_2/N_2 (15:85) mixture gas (green circles). Flow rates are 40 mL min^{-1} and sample temperatures are plotted as blue lines. The sample mass at 150 °C under each gas was normalized to be 0%.

cooled at 296 K for 15 min. An experimental mass change of 5.0% was realized flowing pure CO_2 over the sample and 2.9% in CO_2/N_2 (15:85) mixture gas. This is equal to a CO_2 loading capacity of 1.13 mmol g^{-1} in pure CO_2 and approximately three fifths of this value (0.65 mmol g^{-1}) in flue gas simulant, which emphasizes the capabilities of PCN-200 as a sorbent to remove CO_2 from flue gas.

We solved the crystal structure of the CO_2 loaded phase (PCN-200-CO_2) from in situ SPD data and refined it by the Rietveld method (Figure 4a and Figure 4b, top). The transition from as-synthesized to activated to gas loaded phases

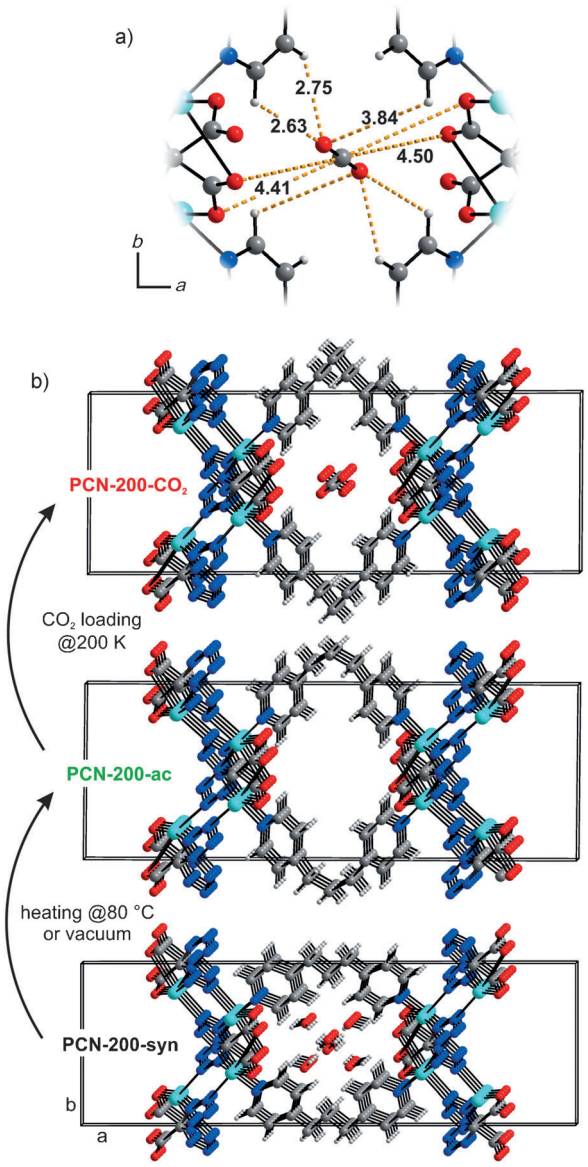

Figure 4. Structural changes of PCN-200 upon activation and CO_2 adsorption obtained by in situ SPD data: a) close-up view of the multipoint bonded CO_2 molecule in the pore. Distances are given in Å; b) perspective view of a single pore in its unit cell along the *c* axis of the as-synthesized (PCN-200-syn, bottom), activated (PCN-200-ac, middle), and CO_2-loaded phase (PCN-200-CO_2, top).

can clearly be seen in the top view of the powder patterns (Figure 5). We used this, the fourth technique, to give us insights to the CO_2 trapping mechanism (for a complete description and more detailed figures of all in situ experiments, see the Supporting Information, Section S3). The crystallographic determination of CO_2 at the center of the pore is confirmed by annealing simulations (Supporting Information, Figure S21) and DFT calculations, which show multipoint CO_2–framework interactions. Based on the simulations, crystal structure and adsorption data, we can exclude molecular sieving as a possible mechanism for the selectivity. The high selectivity can be explained by the special adsorption properties of PCN-200, where all adsorption sites are

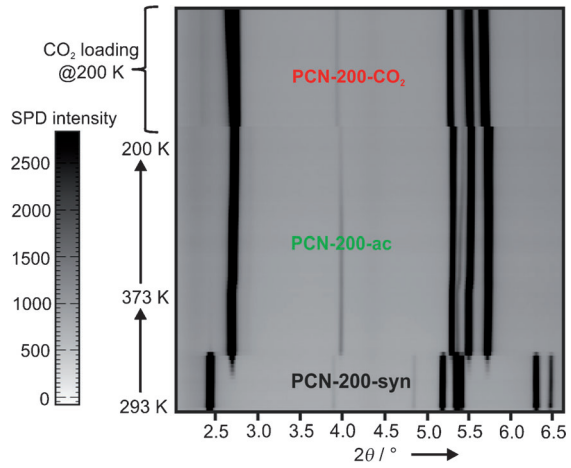

Figure 5. Top view of the in situ temperature- and gas-loading-dependent SPD patterns: upon heating PCN-200-syn, a phase transition is observed, leading to PCN-200-ac. After cooling and CO_2 adsorption, PCN-200-CO_2 is observed.

shared by CO_2 and N_2; CO_2 is heavily favored in competition owing to its stronger interactions with the framework.

The activation and gas loading process can be delineated by following just a few reflections during the in situ SPD experiment, as shown in Figure 6. Upon activation, the (200) reflection is shifted to higher 2θ values (ca. 2.7°) and the two reflections at 5–6° 2θ split into three reflections. Upon gas loading, the intensities become relevant: Depending on the gas loading, the relative intensities of the (200) and the $(1\bar{1}\bar{1})$ at circa 5.3° reflection change. The higher the gas uptake, the less intense the (200) and the more intense the $(1\bar{1}\bar{1})$ reflection, which is evident when comparing the PCN-200-CO_2 patterns at 296 and 200 K. The nearly identical patterns of PCN-200-ac and the N_2 loaded phase again emphasize the disparity between N_2– and CO_2–framework interactions. As is

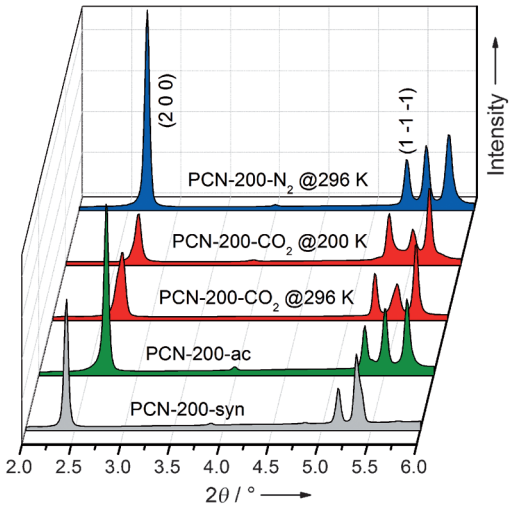

Figure 6. Side view of the in situ temperature- and gas-loading-dependent SPD patterns: after activation of PCN-200-syn (gray), PCN-200-ac (green) was loaded with CO_2 at 296 K and 200 K (red) and N_2 (blue) at 296 K. For different views, see the Supporting Information, Figures S9 and S10.

to be expected from changes in reflection position and intensity, minor changes in unit cell parameters and atom-atom bond distances/angles are also observed (Supporting Information, Tables S3 and S4).

Flexible MOF materials have already been well-described.[6,15] Upon guest removal, those materials show a distinct change in their structures, which leads to a change in their pore volume. This flexible behavior can be traced back to geometric changes in the coordination environment of their metal clusters (SBUs). However, in PCN-200 the transformation from the as-synthesized to the activated form is accompanied by a negligible change in its SBU, but a dramatic change in the conformation of the linking propylene chain of the bipyridyl ligand. This conformation change shrinks the unit-cell volume from 2489 to 2226 Å^3 and opens the kinetic pore diameter from 2.9 to 4.4 Å. Upon CO_2 loading, the overall volume is almost identical; however, a significant change in the unit cell parameters (especially the β angle) can be observed, leading to a distinct change of the pore shape and size in the CO_2 loaded form (compare structures in Figure 4b middle and top). This stimuli-responsive behavior (stimuli = CO_2) is induced by a further reconformation of the propylene chain. The flexibility mechanism for PCN-200 strongly contrasts that of traditional porous MOFs in which the flexibility is based on a change in its SBU. Thus, for a better understanding of this CO_2 trapping effect based on the ligand elasticity in PCN-200, we introduced the term "elastic single-molecule trap".

PCN-200 falls into a new class of compounds which exhibits selectivity based on a novel trapping mechanism. The state-of-the-art MOF, Mg-MOF-74,[12,16] has reported a tremendous CO_2 adsorption capacity (only after energy-intense activation conditions[17]), but the lack of water stability[18] and loss in capacity in consecutive cycles[19] will negatively affect working performance. Although water, like in most other solid porous materials, probably affects the CO_2 loading capacity, PCN-200 is water stable and keeps its porosity upon water contact. We believe that, in an industrial setting, the higher selectivity, stability, and extremely low (re-)activation energy of PCN-200 compared to state-of-the-art materials[20] will prove to be more important factors than a high pure-component loading capacity. Moreover, for scale-up processes, it is worth mentioning that PCN-200 is very easy to synthesize with cheap commercially available reactants in a 95% yield, water-based, one-pot synthesis with no purification steps needed.

In summary, we have shown that we can rationally design a material to recognize a specific guest molecule. PCN-200 was demonstrated, using a variety of methods, to be effective at selectively adsorbing CO_2 over N_2, while being stable to the harsh flue-gas conditions. This is a significant step forward in terms of rationally designing a material for a specific guest interaction. By moving down an entirely new path of tuning interactions by creating precise CO_2 traps, instead of mimicking existing technologies, we have opened up a new avenue of MOF design that can be applied to gas and liquid separations as well as in molecular recognition. Preliminary results show that varying the metal center and ligand length will open up

a new class of stable compounds with interesting physical properties.

Experimental Section

Synthesis of PCN-200: The straightforward synthesis of bulk material with commercially available reactants leads to total synthesis cost according to Alfa Aesar prices of US$4.10/g. Microcrystalline bulk material was prepared by a reaction of $Cu(OAc)_2$ (363.2 mg, 2.0 mmol), sodium ethyl ester tetrazolate-5-carboxylate (NaEttzc, 328.2 mg, 2.0 mmol), and dpp (198.2 mg, 1.0 mmol) in H_2O (15 mL). After stirring this mixture at 150°C for 1 day, the resultant blue precipitate was filtered, washed with H_2O, EtOH, and Et_2O, and dried in air. Yield: 574 mg (95%). The purity was checked by XRPD (Supporting Information, Figure S5). Elemental analysis calcd (%) for $C_{8.5}H_{10}CuN_5O_{3.5}$: C 33.83, H 3.34, N 23.21; found: C 33.63, H 3.30, N 23.30. Blue crystalline plates for single-crystal X-ray diffraction studies were isolated from the reaction of a mixture containing $Cu(OAc)_2$ (36.3 mg, 0.2 mmol), NaEttzc (32.8 mg, 0.2 mmol), dpp (19.8 mg, 0.1 mmol), and H_2O (3 mL) at 100°C for 4 days. Full experimental details are presented in the Supporting Information.

Crystal data from single-crystal diffraction studies for PCN-200-syn: $C_{8.5}H_{10}CuN_5O_{3.5}$, $M_r = 301.76$, monoclinic, space group $C2/c$, $a = 28.612(2)$, $b = 9.3899(7)$, $c = 9.2741(8)$ Å, $\beta = 92.657(10)°$, $V = 2488.9(3)$ Å^3, $Z = 8$, total reflections = 2399, independent reflections = 1688, $R_{int} = 0.0652$, GOF = 0.972, R_1 $[F_0 > 4\sigma(F_0)] = 0.0611$, wR_2 [all data] = 0.1775 (Supporting Information, Section S2).

In situ SPD data were collected at the 1-BM beamline at the Advanced Photon Source, Argonne National Laboratory. Crystal data from SPD studies for PCN-200-ac @296 K: $C_{8.5}H_7CuN_5O_2$, $M_r = 274.7$, monoclinic, space group $C2/c$, $a = 28.697(2)$, $b = 9.2637(5)$, $c = 9.3223(5)$ Å, $\beta = 116.087(4)°$, $V = 2225.8(2)$ Å^3, $Z = 8$, $R_p = 0.0392$, $R_{wp} = 0.0551$, GOF = 4.07, R_{Bragg}, = 0.0472. Crystal data for PCN-200-CO_2 @296 K: $C_{8.875}H_7CuN_5O_{2.75}$, $M_r = 291.2$, monoclinic, space group $C2/c$, $a = 28.561(5)$, $b = 9.3537(18)$, $c = 9.2553(15)$ Å, $\beta = 116.753(10)°$, $V = 2207.9(7)$ Å^3, $Z = 8$, $R_p = 0.0591$, $R_{wp} = 0.0836$, GOF = 5.59, R_{Bragg}, = 0.1367. Crystal data for PCN-200-CO_2 @200 K: $C_9H_7CuN_5O_3$, $M_r = 296.7$, monoclinic, space group $C2/c$, $a = 28.548(6)$, $b = 9.4032(19)$, $c = 9.2876(17)$ Å, $\beta = 117.043(10)°$, $V = 2220.6(8)$ Å^3, $Z = 8$, $R_p = 0.0531$, $R_{wp} = 0.0699$, GOF = 4.77, R_{Bragg}, = 0.1384. Crystal data for PCN-200-N_2 @296 K: $C_{8.5}H_7CuN_5O_2$, $M_r = 296.73$, monoclinic, space group $C2/c$, $a = 28.668(6)$, $b = 9.2413(14)$, $c = 9.2844(15)$ Å, $\beta = 115.953(10)°$, $V = 2211.7(7)$ Å^3, $Z = 8$, $R_p = 0.0365$, $R_{wp} = 0.0508$, GOF = 5.08, R_{Bragg}, = 0.1000 (Supporting Information, Section S3).

CCDC 855255, 855256, 855257, 855258, and 855259 contains the supplementary crystallographic data for this paper. These data can be obtained free of charge from The Cambridge Crystallographic Data Centre via www.ccdc.cam.ac.uk/data_request/cif.

Received: April 18, 2012
Revised: July 26, 2012
Published online: September 3, 2012

Keywords: CO_2 capture · metal–organic frameworks · porous materials · X-ray diffraction

[1] a) S. Chu, *Science* **2009**, *325*, 1599; b) N. MacDowell, N. Florin, A. Buchard, J. Hallett, A. Galindo, G. Jackson, C. S. Adjiman, C. K. Williams, N. Shah, P. Fennell, *Energy Environ. Sci.* **2010**, *3*, 1645 – 1669.
[2] a) G. T. Rochelle, *Science* **2009**, *325*, 1652 – 1654; b) J. P. Ciferno, J. J. Marano, R. K. Munson, *Chem. Eng. Prog.* **2011**, *107*, 34 – 44.
[3] a) D. Zhao, D. J. Timmons, D. Yuan, H.-C. Zhou, *Acc. Chem. Res.* **2011**, *44*, 123 – 133; b) M. Wriedt, C. Näther, *Chem. Commun.* **2010**, *46*, 4707 – 4709; c) C. Janiak, J. K. Vieth, *New J. Chem.* **2010**, *34*, 2366 – 2388.
[4] a) D. M. D'Alessandro, B. Smit, J. R. Long, *Angew. Chem.* **2010**, *122*, 6194 – 6219; *Angew. Chem. Int. Ed.* **2010**, *49*, 6058 – 6082; b) J. R. Li, J. Sculley, H. C. Zhou, *Chem. Rev.* **2011**, *112*, 673 – 1268; c) B. Wang, A. P. Cote, H. Furukawa, M. O'Keeffe, O. M. Yaghi, *Nature* **2008**, *453*, 207 – 211.
[5] a) S. Keskin, T. M. van Heest, D. S. Sholl, *ChemSusChem* **2010**, *3*, 879 – 891; b) J.-R. Li, Y.-G. Ma, M. C. McCarthy, J. Sculley, J.-M. Yu, H.-K. Jeong, P. B. Balbuena, H.-C. Zhou, *Coord. Chem. Rev.* **2011**, *255*, 1791 – 1823; c) R. Vaidhyanathan, S. S. Iremonger, G. K. H. Shimizu, P. G. Boyd, S. Alavi, T. K. Woo, *Science* **2010**, *330*, 650 – 653.
[6] G. Férey, C. Serre, *Chem. Soc. Rev.* **2009**, *38*, 1380 – 1399.
[7] R. S. Haszeldine, *Science* **2009**, *325*, 1647 – 1652.
[8] a) S. Ma, D. Sun, X.-S. Wang, H.-C. Zhou, *Angew. Chem.* **2007**, *119*, 2510 – 2514; *Angew. Chem. Int. Ed.* **2007**, *46*, 2458 – 2462; b) S. Ma, D. Sun, D. Yuan, X.-S. Wang, H.-C. Zhou, *J. Am. Chem. Soc.* **2009**, *131*, 6445 – 6451.
[9] Q.-X. Jia, W.-W. Sun, C.-F. Yao, H.-H. Wu, E.-Q. Gao, C.-M. Liu, *Dalton Trans.* **2009**, 2721 – 2730.
[10] Q.-X. Jia, Y.-Q. Wang, Q. Yue, Q.-L. Wang, E.-Q. Gao, *Chem. Commun.* **2008**, 4894 – 4896.
[11] T. K. Maji, G. Mostafa, R. Matsuda, S. Kitagawa, *J. Am. Chem. Soc.* **2005**, *127*, 17152 – 17153.
[12] J. A. Mason, K. Sumida, Z. R. Herm, R. Krishna, J. R. Long, *Energy Environ. Sci.* **2011**, *4*, 3030 – 3040.
[13] R. H. Weiland, J. C. Dingman, D. B. Cronin, *J. Chem. Eng. Data* **1997**, *42*, 1004 – 1006.
[14] a) P. L. Llewellyn, S. Bourrelly, C. Serre, A. Vimont, M. Daturi, L. Hamon, G. De Weireld, J.-S. Chang, D.-Y. Hong, Y. Kyu Hwang, S. Hwa Jhung, G. r. Férey, *Langmuir* **2008**, *24*, 7245 – 7250; b) T. M. McDonald, D. M. D'Alessandro, R. Krishna, J. R. Long, *Chem. Sci.* **2011**, *2*, 2022 – 2028.
[15] S. Horike, S. Shimomura, S. Kitagawa, *Nat. Chem.* **2009**, *1*, 695 – 704.
[16] S. R. Caskey, A. G. Wong-Foy, A. J. Matzger, *J. Am. Chem. Soc.* **2008**, *130*, 10870 – 10871.
[17] J. Liu, A. I. Benin, A. M. B. Furtado, P. Jakubczak, R. R. Willis, M. D. LeVan, *Langmuir* **2011**, *27*, 11451 – 11456.
[18] A. C. Kizzie, A. G. Wong-Foy, A. J. Matzger, *Langmuir* **2011**, *27*, 6368 – 6373.
[19] D. Britt, H. Furukawa, B. Wang, T. G. Glover, O. M. Yaghi, *PANS* **2009**, *106*, 20637 – 20640.
[20] Y.-S. Bae, R. Q. Snurr, *Angew. Chem.* **2011**, *123*, 11790 – 11801; *Angew. Chem. Int. Ed.* **2011**, *50*, 11586 – 11596.

